ACS APPLIED MATERIALS & INTERFACES

www.acsami.org

Research Article

Polymer Patterning by Laser-Induced Multipoint Initiation of Frontal Polymerization

Andrés L. Cook, Mason A. Dearborn, Trevor M. Anderberg, Kavya Vaidya, Justin E. Jureller, Aaron P. Esser-Kahn,* and Allison H. Squires*

Cite This: https://doi.org/10.1021/acsami.4c00216

Read Online

ACCESS | Metrics & More | Article Recommendations | Supporting Information

ABSTRACT: Frontal polymerization (FP) is an approach for thermosetting plastics at a lower energy cost than an autoclave. The potential to generate simultaneous propagation of multiple polymerization fronts has been discussed as an exciting possibility. However, FP initiated at more than two points simultaneously has not been demonstrated. Multipoint initiation could enable both large-scale material fabrication and unique pattern generation. Here, the authors present laser-patterned photothermal heating as a method for simultaneous initiation of FP at multiple locations in a 2-D sample. Carbon black particles are mixed into liquid resin (dicyclopentadiene) to enhance absorption of light from a Ti:sapphire laser (800 nm) focused on a sample. The laser is time-shared by rapid steering among initiation points, generating polymerization using up to seven simultaneous points of initiation. This process results in the formation of both symmetric and asymmetric seam patterns resulting from the collision of fronts. The authors also present and validate a theoretical framework for predicting the seam patterns formed by front collisions. This framework allows the design of novel patterns via an inverse solution for determining the initiation points required to form a desired pattern. Future applications of this approach could enable rapid, energy-efficient manufacturing of novel composite-like patterned materials.

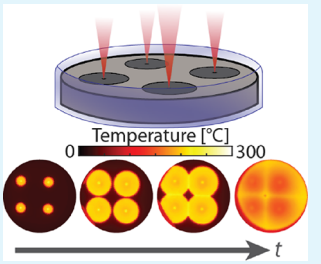

KEYWORDS: *frontal polymerization, patterned materials, photothermal initiation, laser initiation, dicyclopentadiene*

INTRODUCTION

Frontal polymerization (FP)[1,2] is an energy-efficient alternative manufacturing mode for thermoset polymers and composites, which require large amounts of energy for thermal processing in a pressurized autoclave.[3] In contrast, FP is a self-propagating polymerization reaction that requires only a small, localized energy input for initialization, typically delivered by a heated tip or wire.[2,4,5] After initiation, heat is generated by the exothermic polymerization reaction and propagated by conduction and convection.[4,6] FP was initially described using acrylate chemistry, but it has since been demonstrated using many other monomers, although largely within the acrylate family.[4] In this work, we focus on polymerizing dicyclopentadiene (DCPD), in which FP proceeds by frontal ring-opening metathesis polymerization (FROMP).[7−9]

Beyond its potential advantages for energy efficiency, FP can also be used to produce patterned polymers with spatially varying material properties.[10−17] To date, the best-characterized means of FP pattern creation have used single fronts to create non-uniformity, multiple materials to create a copolymer or composite,[11,12,15] or modulation of the front (or material[18]) to pattern a single polymer.[10,13,14,17,19] Less explored is the use of multiple fronts in patterning, which prior review work has identified as a target for future development of FP technology.[4] When two fronts meet, they form a seam at the collision zone.[20] Seams reach a higher maximum temperature than the surrounding polymer,[21,22] which can induce changes in their material properties relative to the bulk.[14] Modulated temperature at seam locations allows for spatially controlled energy deposition. More colliding fronts would allow more complex patterning, so increasing the number of possible initiation points would represent a major breakthrough in FP patterning. However, the position of a seam depends on the difference between the initiation times of the colliding fronts. Multipoint patterning is therefore limited by the uniformity of initiation times, which becomes increasingly difficult with more initiation points. Because of these limitations, multipoint patterning of FP with more than two initiation points has not previously been reported.

Photoinitiation is a promising route to overcome challenges in implementing multipoint initiation because light can be readily patterned onto a substrate to achieve concurrent rather than sequential initiation at multiple locations. To date, light has been used to trigger FP either using a photoinitiator that chemically or thermally triggers polymerization[23−28] or using direct absorption of light by the sample.[29−32] Lasers offer high levels of power per unit area. This capability has enabled

Received: January 4, 2024
Revised: February 12, 2024
Accepted: February 16, 2024

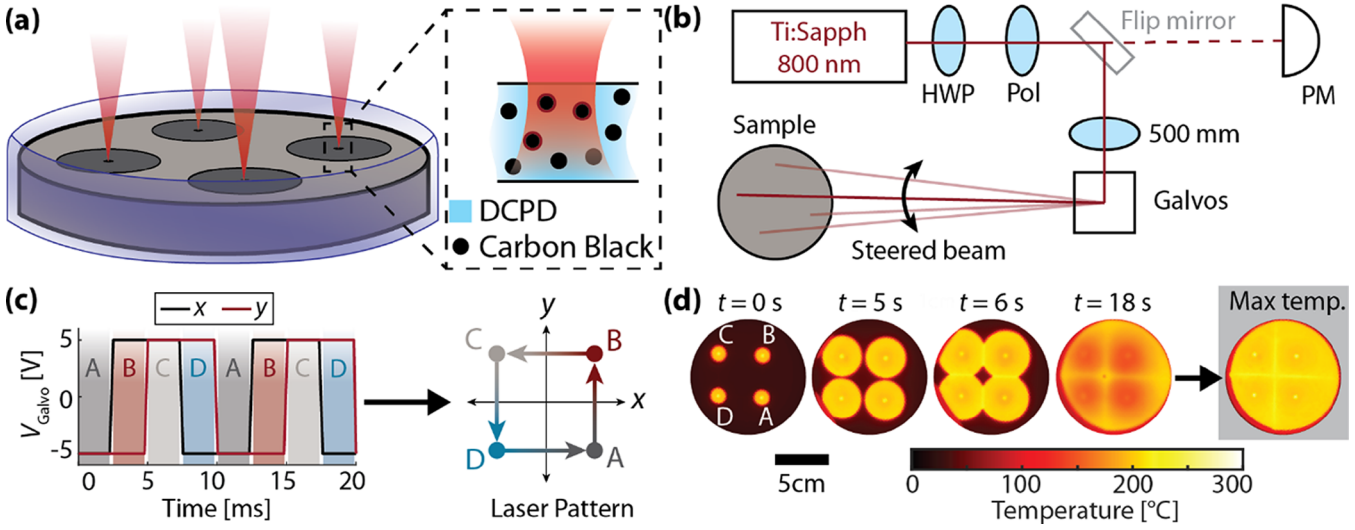

Figure 1. Overview of multipoint frontal polymerization. (a) Illuminating carbon black-doped DCPD from above with a near-IR laser causes rapid heating, followed by initiation of FP. (b) Schematic of the optical apparatus for steering the focused laser beam on the sample. The beam first passes through a half-wave plate (HWP) and polarizer (Pol), decreasing its power according to the wave plate angle. It can then be directed either into a power meter or through a lens (focal length 500 mm) and into a pair of movable galvanometer mirrors (Galvos). The laser is then directed onto the sample by an overhead mirror. (c) Illustration of beam time-sharing by galvos. Left: Input voltage signals are plotted as a function of time for x and y galvo mirrors. Right: The path of the beam is a parametric curve in the x–y plane, as created by the time-dependent voltage signals. (d) Frames from a thermal video of four-point polymerization showing fronts propagating and colliding with one another. The far-right panel shows the maximum temperature of each pixel over time, showing that seams polymerize at a higher temperature than the bulk.

demonstration of photoinitiation of FP from a distance,[30−33] which has also been accomplished using an electromagnetic field.[34] In principle, lasers can also offer precise spatiotemporal control of the beam by steering from a distance with galvanometer mirrors or acousto-optic deflectors. A steered laser beam could be programmed to pause at each of several desired initiation locations arranged in any geometric pattern, enabling highly reproducible photoinitiation patterning. This approach contrasts with patterned FP by resistive heating, where each wire operates independently and must be mechanically placed at the initiation location.

Here, we accomplish multipoint initiation in DCPD for up to 7 points using a focused, steered laser beam time-shared among initiation points. We employed carbon black to assist photothermal initiation via increased heat absorbance of patterned near-IR laser illumination. To enable optimization of laser-patterned multipoint FP initiation, we first characterized front initiation and propagation parameters for varying optical and geometric conditions. We demonstrated that the synchronicity of our laser initiation approach allows us to reduce the seam positioning error to far below one seam width. Features of the composite resulting from front intersections, including seams and peaks, are governed by the geometry of the initiation pattern. We developed a geometric framework for understanding and predicting these features for any given pattern of initiation points. We apply this framework to the inverse problem to determine the initiation point pattern that will produce a desired set of seams. Finally, we demonstrate that our initiation mechanism also allows us to use advanced initiation methods, including asynchronous and nonpunctate initiation patterns. This work is the first instance of simultaneous FP initiated at more than two points and presents new opportunities for FP-based polymer patterning and manufacturing.

MATERIALS AND METHODS

Sample Preparation. The monomer preparation procedure was derived from Robertson et al.[2] 5-Ethylidene-2-norbornene (ENB) was added as a stabilizing agent to prevent DCPD from solidifying at room temperature. We added 625.7 μL of phenylcyclohexane (PCH) to 256.8 μg of second-generation Grubbs catalyst (GC2) and sonicated for 20 min to dissolve, after which 37.2 μL of tributyl phosphite (TBP) was added as an inhibitor and mixed by inversion. The combined catalyst and inhibitor were dispensed into 626 μL aliquots and stored at −4 °C prior to use.

Prior to polymerization, 950 mg of carbon black was added to 20 mL of stabilized monomer and sonicated for 20 min, with manual stirring after 10 and 20 min of sonication. The sample was then stored short-term in a rotary mixer to keep the carbon black suspended until polymerization (no longer than 2 h). Immediately before polymerization, the thawed catalyst/inhibitor was added to the monomer, mixed by inversions, and poured into a 10 cm-diameter Petri dish (Corning 3160102BO). The thickness of the poured sample prior to polymerization was approximately 2.5 mm.

Laser Apparatus. The optical setup for photothermal initiation depicted in Figure 1b shows near-IR laser illumination passing through power and position control optics to bring it to the sample plane. The light source is a Coherent Chameleon Ultra Titanium:sapphire 800 nm pulsed laser. Immediately prior to polymerization (after combining the monomer and catalyst), we read the laser power with a power meter placed on an alternate beam path (accessible via a flip mirror). The laser passes through a 500 mm focal length lens that focuses the beam to a 0.25 mm-wide point on the surface of the sample.

To control the position of the beam, we sent the laser through a Thorlabs QS15XY dual galvanometer mirror, one controlling each axis of motion, controlled by an Arduino microcontroller (Arduino Nano). The galvos are driven by a pair of −5 to 5 V analog electrical signals (one per axis), while the Arduino outputs a pair of digital signals representing two numbers between 0 and 4095 inclusive. To mediate between these two signals, we built a custom "predriver" board composed of a digital-analog converter (DAC) and an amplifier for each axis. The DAC converts the digital signal to an analog signal between 0 and 5 V, which the amplifier converts to the −5 to 5 V

https://doi.org/10.1021/acsami.4c00216
ACS Appl. Mater. Interfaces XXXX, XXX, XXX−XXX

range required by the galvos. Through these electronics, we can represent points on the sample as pairs of integers between 0 and 4095. Patterns are programmed into the Arduino as three separate lists. The first two lists store the x and y coordinates of each point in the sequence, while the third list stores the dwell time. The Arduino then iterates through the lists, holding each (x, y) position for the specified time. When the end of the list is reached, the control software loops back to the beginning. Because the galvo controls the angle of the beam rather than its position (in the plane transverse to the beam), the scaling of the galvo signal to the $x-y$ positions on the sample depends upon the distance between the galvos and the sample.

Temperature Measurement. Temperatures were recorded with an FLIR E8 infrared camera mounted above the sample. For each video, frames were exported from FLIR ResearchIR software to a stack of .csv files (one per frame) containing temperature values (16-bit floating point) that were imported into MATLAB for analysis.

Height Profiling and Imaging. Height profiles and dark-field top-down images of polymerized samples were taken on an Olympus DSX1000 microscope. Volume estimates were made with the LEXT OLS5100 analysis application.

Analysis. *Image Scaling.* To determine the appropriate pixel-to-millimeter scale factor, the diameter of the dish (10 cm) was used as a reference. Because images were acquired from above, obliquity did not affect the scaling. In cases where the Olympus microscope was used (i.e., height maps and dark-field images), the instrument provided a scale bar.

Front Speed. To determine the speed of the front, we first determined its displacement by measuring the area enclosed by a front and converting to the equivalent radius of a circle $\left(r = \sqrt{\frac{A}{\pi}}\right)$. This approximation has the effect of averaging over directions and limiting the effects of anisotropic front propagation. Front velocity is calculated by differentiating the front radius with respect to time.

RESULTS

Programmable Laser-Ignited Frontal Polymerization. In developing a method to create complex and precise patterns of seams in DCPD, we used a pulsed Ti:sapphire laser tuned to 800 nm to heat the monomer, which is doped with carbon black to increase light absorption (Figure 1a). We coupled this laser to a pair of galvanometer mirrors to allow us to rapidly change the position of the beam (Figure 1b). By steering the laser focus quickly among multiple initiation points with dwell times of 1−5 ms each, we can effectively time-share the beam power, as shown in Figure 1c. This results in fast, synchronized multipoint initiation of FP, as demonstrated in the thermal snapshots of Figure 1d. After initiation, the fronts move outward radially until they collide, polymerizing the entire sample. As expected, the seams where fronts collide reach higher maximum temperatures than the surrounding polymer, indicating that seam patterning corresponds to patterning of thermal energy within the material.

Characterizing Laser-Ignited FP. To quantify the rapidity and synchronicity of initiation, we measured initiation onset time and time between initiation points.[28,29] Figure 2a shows the time to FP initiation as a function of applied laser power for a series of single-point tests. As the power increases, the initiation time converges toward zero. These data are well fitted by a simple model where initiation occurs once the energy of the sample has been raised by a fixed threshold energy ΔE_{thresh} so that the time to initiation t is inversely proportional to the initiation power P:

$$t = \frac{\Delta E_{thresh}}{P} \quad (1)$$

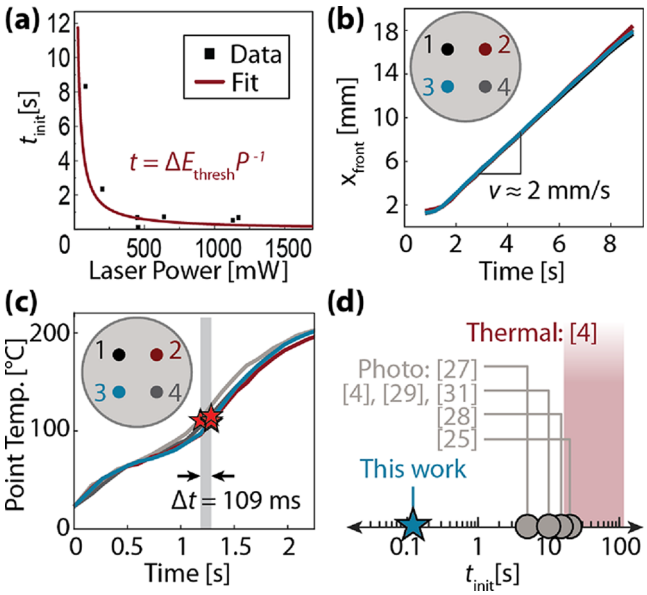

Figure 2. Characterization of multipoint FP. (a) Time to initiation vs illumination power, along with the reciprocal fit curve. The fit indicates a fixed energy for initiation of 294 mJ. (b) Front position as a function of time for four simultaneously ignited fronts, showing a constant front velocity of 2 mm s^{-1}. (c) Initiation point temperature vs time for a four-point initiation. Red stars indicate the identified initiation times. (d) Photoinitiation times from the literature (gray and red) and our work (blue). Where multiple initiation times were described in a reference, the shortest is plotted here.

The constant of proportionality is the threshold energy, ΔE_{thresh}, required to initiate FP. Here, a weighted fit to our data gives a value of $\Delta E_{thresh} = 294 \pm 108$ mJ. For more details regarding the trend shown in Figure 2a, see SI Note 1.

The required synchronicity for patterning depends upon the front propagation speed and the desired placement precision of features, such as seams. In our system, the front propagation speeds are nearly identical within each sample at approximately 2 mm s^{-1} (Figure 2b). Therefore, reproducible feature placement (i.e., seam position deviations of less than one seam width) requires synchronicity of FP initiation within ~1 s given our seam widths of ~1 mm (see SI Note 2 and Figures S3 and S4). The measured synchronicity of our setup is on the order of tenths of a second (seam placement precision, ~0.1 mm). To demonstrate this, Figure 2c shows temperature traces at each of four initiation points during illumination. An initial sharp temperature rise plateaus slowly, followed by FP initiation at about 1.25 s (gray band), with exact initiation times calculated as described in SI Note 1. Here, polymerization is initiated at all points within 0.11 s. For further discussion of the causes of asynchronicity, see SI Note 3. Beyond its advantages in initiation speed, laser-ignited multipoint FP is also highly synchronous.

Rapid initiation is helpful for patterning, as it increases synchronicity and reduces diffusive preheating of the monomer surrounding the initiation points. In comparing our method with the literature, we noted that our laser-based method initiated FP much more rapidly than did other light-based setups. Representative initiation times from previous photoinitiation studies are shown in Figure 2d. Our approach decreases the initiation time by over an order of magnitude while retaining the ability to initiate at many individual, arbitrarily patterned points.

https://doi.org/10.1021/acsami.4c00216
ACS Appl. Mater. Interfaces XXXX, XXX, XXX−XXX

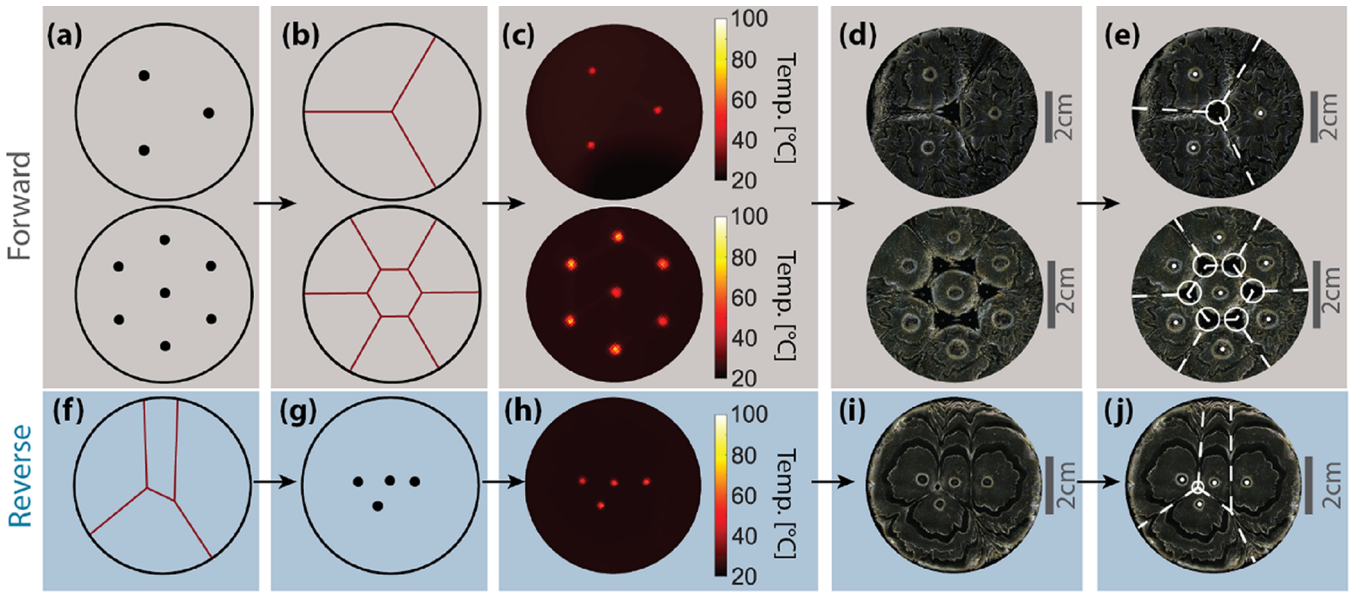

Figure 3. Process for forming a multipoint FP pattern. (a) Desired initiation pattern. (b) Predicted seam pattern. (c) IR image of the initiation points. (d) Dark-field camera image of the FP result. (e) Camera image annotated with seams (dashed lines), initiation points (closed circles), and peaks (open circles). Panels (f)−(j) show the inverse Voronoi algorithm to produce an initiation pattern from a desired seam pattern. The first two panels are therefore reversed from panels (a) and (b).

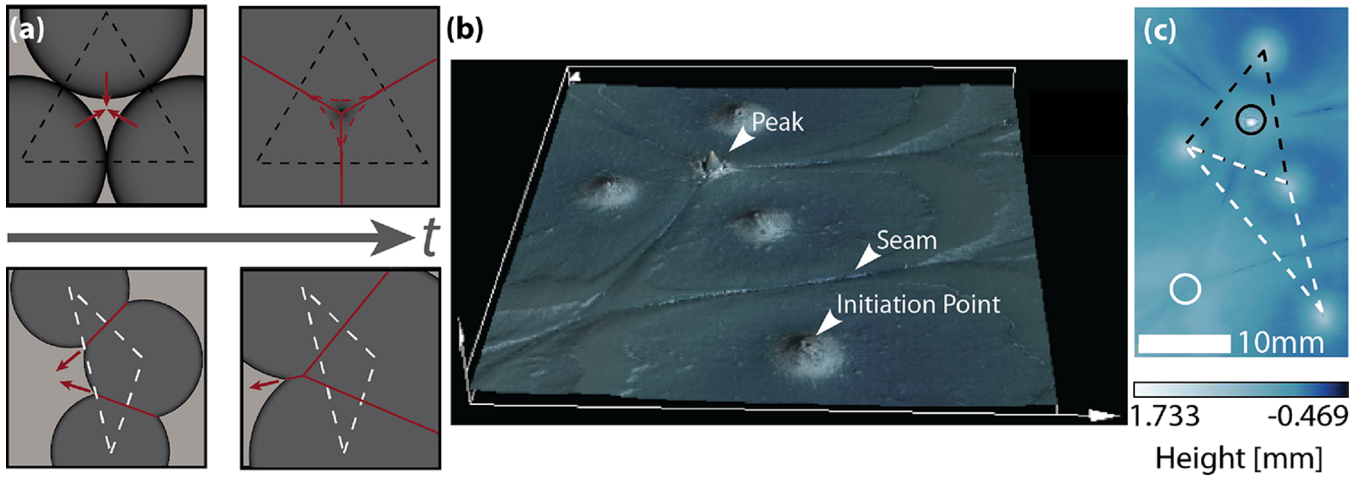

Figure 4. Characterization of surface patterns induced by multipoint FP. (a) Cartoon schematic of peak formation, showing seams forming (red) as monomer is pushed away from the fronts (red arrows). Dashed triangles connect the initiation points involved in seam convergence. (b) 3D scan of a sample showing two seam convergences, one with and one without a peak (false color overlay indicates height) (not tilt-corrected). The image region is 36 mm wide (horizontal page axis) and 39 mm high (vertical page axis). (c) Height map of the sample from panel (b). An acute triangle (black) results in a peak when the seams intersect inside the triangle, while an obtuse triangle (white) does not lead to a peak.

Controllable Seam Patterning with Multipoint FP. To understand how multipoint FP generates geometric patterns, we developed a model based on the geometry of the initiation points. Two example geometries that we tested are shown in Figure 3a, one with three points (top) and one with seven points (bottom). Under the assumption that polymerization fronts propagate radially outward at constant and equal speeds, as was observed in early tests (Figure 2b), we can predict where seams will form. When polymerization is initiated simultaneously at multiple points, pairs of fronts will first intersect at the midpoint between their corresponding initiation points. As the fronts continue to propagate, they meet at points equidistant from each initiation point: the perpendicular bisector of the initiation points. When more than two initiation points are present, the perpendicular bisectors form a network called a Voronoi diagram. Therefore, using the initiation point geometries from Figure 3a, we predicted that seams would form at the locations indicated in Figure 3b.

Having developed our model, we then verified it experimentally. We implemented both the three- and seven-point patterns from Figure 3a with the initiation patterns shown in the thermal images in Figure 3c. Dark-field images of the resulting polymerized samples are shown in Figure 3d, illustrating that the seam patterns match the predicted locations. In addition to seams, we noticed the formation of peaks in the sample at locations where three fronts collided as well as some minor rippling features, both of which are evident from contrast changes in the digital image. Figure 3e shows the measured locations of all of the initiation points, seams, and

https://doi.org/10.1021/acsami.4c00216
ACS Appl. Mater. Interfaces XXXX, XXX, XXX−XXX

peaks superimposed on the image. These results can be extrapolated to the more general observation that, mathematically, any set of initiation points result in a seam pattern that can be modeled and predicted using a Voronoi diagram. For additional camera images of polymerized samples, see Figure S2.

The inverse problem is to derive the initiation point locations required to produce a desired seam pattern, such as the one shown in Figure 3f. Using a geometric algorithm for inverse Voronoi diagrams,[35] we predicted that this seam pattern could be produced by the set of initiation points shown in Figure 3g. We then implemented this pattern, as shown in the thermal image in Figure 3h, which resulted in the correct polymerized sample pattern shown in Figure 3i. Measured locations of all initiation points, seams, and peaks are superimposed onto the digital image in Figure 3j. In contrast to the forward prediction problem, not all desired seam patterns can be realized by FP because not all sets of connected line segments form Voronoi diagrams. Moreover, some desired seam patterns have degenerate inverse solutions (SI Note 3).

Controllable Peak Patterning with Multipoint FP. As seams form, they can collide with each other to form new structures at their intersections, as depicted in Figure 4a. Because fronts propagate at equal speeds, this intersection will be located at the point equidistant from all initiation points involved, i.e., their circumcenter. If the circumcenter is inside of the polygon formed by the initiation points, then the expanding fronts will enclose a "trapped volume" before they all converge at the center (top panels of Figure 4a). As the trapped volume contracts, we hypothesize that unreacted monomer is pushed ahead of the front and into the center, forming a peak at the intersection. We expect to see peaks formed only when the initiation points form a polygon that contains its circumcenter. Otherwise, two seams will collide and form a third seam, with no peak present, as depicted in the bottom panels of Figure 4a. Our success in predicting and patterning seam locations also allowed us to predict and pattern the locations of elements that are formed by the intersections of seams.

To demonstrate the principles of peak formation, we examined a sample that shows both peaked and nonpeaked seam collisions. A 3-D profile of this sample shows major surface features, including seams, peaks, and initiation points (Figure 4b). The four initiation points shown form two triangles, one acute and one obtuse (Figure 4c). Because acute triangles contain their circumcenters while obtuse triangles do not, we expect to see a peak at the acute circumcenter and no peak at the obtuse circumcenter, as borne out by our experimental results and illustrated in the height map (Figure 4c, circles). Based on our model, only patterns with straight seams are achievable with simultaneous multipoint FP initiation, and the geometry of initiation points is dictated by formation of seams at midpoints between them.

Asynchronous and Nonpunctate FP Initiation Patterns. Asynchronous multipoint initiation could provide access to more complex patterns. While this technique pushes the limits of our current abilities, we can demonstrate a simple example experimentally. When we initiate polymerization at two points at different times, the fronts will no longer meet along a straight line. Instead, the seam will form at points where the distance to one initiation point is equal to the distance to the other initiation point, plus a fixed offset $v_f\Delta t$, where v_f is the front speed and Δt is the delay in initiation times. This condition defines a hyperbola bending around the point that initiates later. To demonstrate this effect, we performed an asynchronous initiation of two points by increasing the time per galvo cycle spent on one initiation point relative to another, as shown in Figure 5a. As expected, the resulting seam forms a hyperbola.

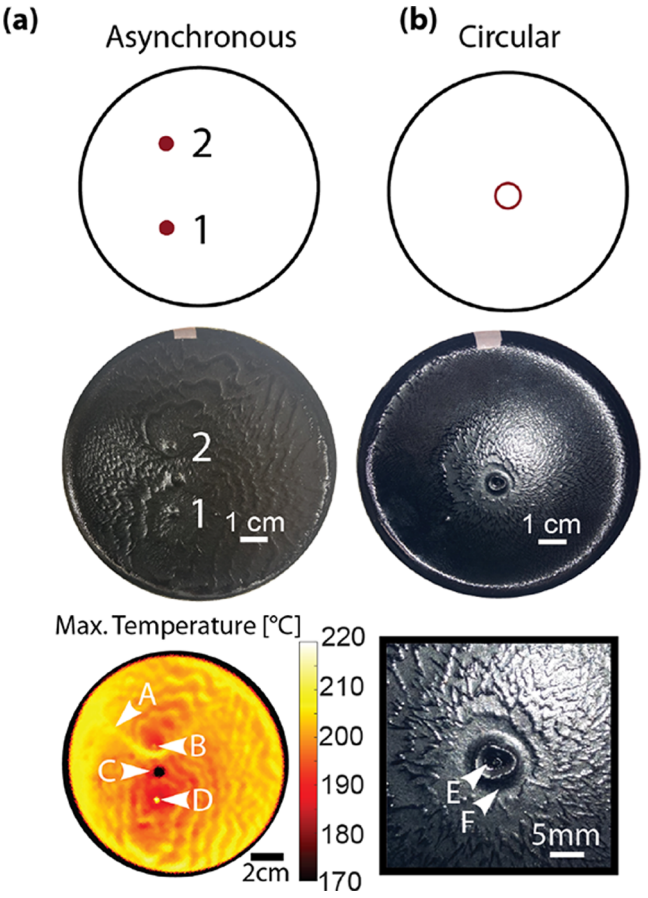

Figure 5. Asynchronous and circular initiation. (a) Asynchronous initiation at points 1 and 2 (left column). (b) Circular initiation (right column). Top row: initiation point patterns. Middle row: camera images of the resulting sample. Bottom row: significant features of the samples. Left: maximum temperature map showing a hyperbolic seam. Right: close-up of the circular initiation site. Labeled points: A, hyperbolic seam; B, second initiation point; C, carbon black cluster; D, first initiation point; E, inner peak; F, initiation ring.

Similarly, nonpunctate initiation patterns also have the potential to generate complex seam and peak patterns. To generate a line or curve of initiation rather than a point, we smoothly scan the galvos by feeding each motor a (sampled) continuous function and uniformly heating a contour. We implemented this for a circular path, producing both an outward-propagating front and an inward-propagating front that forms a peak at the ring's center. The resulting polymer sample is shown in Figure 5b; it is unclear why the ring is distorted from the circle projected by the laser. Together, the ability to apply nonpunctate and asynchronous patterns to initiate FP substantially expands the range of complexity that can be patterned in the resulting material.

https://doi.org/10.1021/acsami.4c00216
ACS Appl. Mater. Interfaces XXXX, XXX, XXX−XXX

DISCUSSION AND CONCLUSIONS

Multipoint FP has great potential for producing patterned materials but has previously been limited by poor synchronicity. Here, we demonstrate a new approach for photothermal initiation by patterning a focused laser beam on a sample, allowing us to initiate polymerization simultaneously at up to 7 points much more rapidly than previously reported (<1 s initiation time, ~0.1 s timing precision). Aside from its speed, our laser-ignited FP is well controlled, with synchronous initiation and steady front speeds. Because of this controllability, we can reduce seam positioning error due to asynchronicity to about 0.1 mm, far less than one seam width. We can also describe the behavior of the fronts with simple rules that allow us to design complex new patterns. These designs can be implemented rapidly due to the flexibility of time-shared laser ignition, providing a fast iterative design loop for patterned polymer manufacturing.

While we can initiate multipoint FP with unprecedented precision, our approach is not without limitations. Synchronicity is limited by the stochastic nature of initiation (see Figure 2). This is potentially due to poor sample mixing, flow conditions during heating, or the presence of carbon black clusters within the sample. The carbon black itself also limits the optical properties of the polymers and increases the viscosity of the monomer mix. Additionally, the time-sharing system used to split the beam limits the number of points that can be accessed before the laser's power is spread too thin to initiate quickly. Consistent with other FP studies, different batches of the monomer and catalyst often result in different surface artifacts (such as ripples and pulses).

Prior studies have demonstrated that higher FP front temperatures correspond to altered material properties.[14] Our observation that maximum temperatures on our samples vary with the same geometry as the seam and peak patterns therefore suggests that material properties of the sample near these features might similarly be altered. Since properties of a composite material are derived from both the component polymer structures and the arrangement of those structures, our multipoint FP approach could in principle be used to confer complex mechanical and material properties for polymer composites in the future.

Other future avenues of multipoint FP research should focus on either characterizing existing multipoint processes or expanding the space of constructible patterns. While our initiation time study (Figure 2b) was conducted with single-point initiation, a similar study on multipoint initiation could provide more insight into the underlying energetics. Similarly, an investigation of the initiation point temperature profiles may explain the anomalies described in SI Note 3. To expand our existing space of patterns, future studies can better define patterning rules and inverse algorithms for asynchronous and nonpunctate initiation. Additionally, our framework currently assumes a planar sample, but the geometry would become substantially more complex on a curved surface. A differential-geometric approach would allow new patterns to be created on nonflat surfaces.

Multipoint FP has broad applications in polymer manufacturing. Seam patterning might be used directly to create inhomogeneous materials with composite properties despite having uniform chemical composition. We can also exploit the uneven distribution of thermal energy to power secondary processes, from chemical reactions to the deformation of shape-memory alloys. Furthermore, laser-ignited multipoint initiation can be used outside of patterning to polymerize objects too large for a single front, or heat deposition can be altered dynamically as part of a front-control feedback loop, such as that designed by Schaer and Bretl.[36] Multipoint initiation, previously inaccessible, is now opening up new opportunities in component manufacturing and design, expanding the potential of FP-based methods.

ASSOCIATED CONTENT

Data Availability Statement

Raw and figure data are available from the corresponding authors upon reasonable request.

Supporting Information

The Supporting Information is available free of charge at https://pubs.acs.org/doi/10.1021/acsami.4c00216.

Initiation time calculation; pattern invertibility; synchronicity of initiation; sample photos (PDF)

AUTHOR INFORMATION

Corresponding Authors

Aaron P. Esser-Kahn − *Pritzker School of Molecular Engineering, University of Chicago, Chicago, Illinois 60637, United States; Institute for Biophysical Dynamics, University of Chicago, Chicago, Illinois 60637, United States;* orcid.org/0000-0003-1273-0951; Email: aesserkahn@uchicago.edu

Allison H. Squires − *Pritzker School of Molecular Engineering, University of Chicago, Chicago, Illinois 60637, United States; Institute for Biophysical Dynamics, University of Chicago, Chicago, Illinois 60637, United States;* orcid.org/0000-0002-2417-1432; Email: asquires@uchicago.edu

Authors

Andrés L. Cook − *Department of Physics, University of Chicago, Chicago, Illinois 60637, United States;* orcid.org/0000-0002-6044-2412

Mason A. Dearborn − *Pritzker School of Molecular Engineering, University of Chicago, Chicago, Illinois 60637, United States*

Trevor M. Anderberg − *Department of Physics, University of Chicago, Chicago, Illinois 60637, United States*

Kavya Vaidya − *Pritzker School of Molecular Engineering, University of Chicago, Chicago, Illinois 60637, United States*

Justin E. Jureller − *James Franck Institute, University of Chicago, Chicago, Illinois 60637, United States;* orcid.org/0000-0001-5760-2385

Complete contact information is available at: https://pubs.acs.org/10.1021/acsami.4c00216

Notes

The authors declare no competing financial interest.

ACKNOWLEDGMENTS

The authors acknowledge valuable discussions and feedback from Kepler Domurat-Sousa, Katie Kloska, Samantha Livermore, Yixiao Dong, Farsa Ram, and Sarah Brown. A.H.S., A.P.E.-K., and J.E.J. acknowledge support from NSF QLCI QuBBE grant OMA-2121044. A.P.E.-K. acknowledges support from AFOSR FA9550-18-1-0229 and FA9550-20-1-0194. A.H.S. acknowledges support from the Neubauer Family Foundation. This work made use of the shared facilities at the

University of Chicago Materials Research Science and Engineering Center, supported by the National Science Foundation under award number DMR-2011854.

REFERENCES

(1) Abliz, D.; Duan, Y.; Steuernagel, L.; Xie, L.; Li, D.; Ziegmann, G. Curing Methods for Advanced Polymer Composites - A Review. *Polym. Polym. Compos.* **2013**, *21* (6), 341−348.
(2) Robertson, I. D.; Yourdkhani, M.; Centellas, P. J.; Aw, J. E.; Ivanoff, D. G.; Goli, E.; Lloyd, E. M.; Dean, L. M.; Sottos, N. R.; Geubelle, P. H.; Moore, J. S.; White, S. R. Rapid Energy-Efficient Manufacturing of Polymers and Composites via Frontal Polymerization. *Nature* **2018**, *557* (7704), 223−227.
(3) Timmis, A. J.; Hodzic, A.; Koh, L.; Bonner, M.; Soutis, C.; Schäfer, A. W.; Dray, L. Environmental Impact Assessment of Aviation Emission Reduction through the Implementation of Composite Materials. *Int. J. Life Cycle Assess.* **2015**, *20* (2), 233−243.
(4) Suslick, B. A.; Hemmer, J.; Groce, B. R.; Stawiasz, K. J.; Geubelle, P. H.; Malucelli, G.; Mariani, A.; Moore, J. S.; Pojman, J. A.; Sottos, N. R. Frontal Polymerizations: From Chemical Perspectives to Macroscopic Properties and Applications. *Chem. Rev.* **2023**, *123* (6), 3237−3298.
(5) Chechilo, N.; Khvilivitskii, R.; Enikolopyan, N. *Dokl Akad Nauk SSSR* **1972**, *204*, 1180−1181.
(6) Gao, Y.; Paul, J. E.; Chen, M.; Hong, L.; Chamorro, L. P.; Sottos, N. R.; Geubelle, P. H. Buoyancy-Induced Convection Driven by Frontal Polymerization. *Phys. Rev. Lett.* **2023**, *130* (2), No. 028101.
(7) Mariani, A.; Fiori, S.; Chekanov, Y.; Pojman, J. A. Frontal Ring-Opening Metathesis Polymerization of Dicyclopentadiene. *Macromolecules* **2001**, *34* (19), 6539−6541.
(8) Ruiu, A.; Sanna, D.; Alzari, V.; Nuvoli, D.; Mariani, A. Advances in the Frontal Ring Opening Metathesis Polymerization of Dicyclopentadiene. *J. Polym. Sci. Part Polym. Chem.* **2014**, *52* (19), 2776−2780.
(9) Robertson, I. D.; Pruitt, E. L.; Moore, J. S. Frontal Ring-Opening Metathesis Polymerization of Exo-Dicyclopentadiene for Low Catalyst Loadings. *ACS Macro Lett.* **2016**, *5* (5), 593−596.
(10) Dearborn, M. A.; Hemmer, J.; Wang, Z.; Esser-Kahn, A. P.; Geubelle, P. H. Controllable Frontal Polymerization and Spontaneous Patterning Enabled by Phase-Changing Particles. *Small* **2021**, *17* (42), 2102217.
(11) Majhi, S. S.; Yadav, N.; Chakraborty, A. K. Development of Periodic Colored Bands via Frontal Polymerization. *J. Indian Chem. Soc.* **2022**, *99* (10), No. 100721.
(12) Fiori, S.; Mariani, A.; Ricco, L.; Russo, S. Interpenetrating Polydicyclopentadiene/Polyacrylate Networks Obtained by Simultaneous Non-Interfering Frontal Polymerization. *E-Polym.* **2002**, *2* (1). DOI: 10.1515/epoly.2002.2.1.404.
(13) Gao, Y.; Dearborn, M. A.; Vyas, S.; Kumar, A.; Hemmer, J.; Wang, Z.; Wu, Q.; Alshangiti, O.; Moore, J. S.; Esser-Kahn, A. P.; Geubelle, P. H. Manipulating Frontal Polymerization and Instabilities with Phase-Changing Microparticles. *J. Phys. Chem. B* **2021**, *125* (27), 7537−7545.
(14) Lloyd, E. M.; Feinberg, E. C.; Gao, Y.; Peterson, S. R.; Soman, B.; Hemmer, J.; Dean, L. M.; Wu, Q.; Geubelle, P. H.; Sottos, N. R.; Moore, J. S. Spontaneous Patterning during Frontal Polymerization. *ACS Cent. Sci.* **2021**, *7* (4), 603−612.
(15) Nuvoli, D.; Alzari, V.; Pojman, J. A.; Sanna, V.; Ruiu, A.; Sanna, D.; Malucelli, G.; Mariani, A. Synthesis and Characterization of Functionally Gradient Materials Obtained by Frontal Polymerization. *ACS Appl. Mater. Interfaces* **2015**, *7* (6), 3600−3606.
(16) Maugeri, D.; Sangermano, M.; Leterrier, Y. Radical Photoinduced Cationic Frontal Polymerization in Porous Media. *Polym. Int.* **2021**, *70* (3), 269−276.
(17) Alzate-Sanchez, D. M.; Cencer, M. M.; Rogalski, M.; Kersh, M. E.; Sottos, N.; Moore, J. S. Anisotropic Foams via Frontal Polymerization. *Adv. Mater.* **2022**, *34* (8), 2105821.
(18) Kumar, A.; Dean, L. M.; Yourdkhani, M.; Guo, A.; BenVau, C.; Sottos, N. R.; Geubelle, P. H. Surface Pattern Formation Induced by Oscillatory Loading of Frontally Polymerized Gels. *J. Mech. Phys. Solids* **2022**, *168*, No. 105055.
(19) Dearborn, M. A. Spontaneous Patterning Via Frontal Polymerization. Ph.D., The University of Chicago, United States -- Illinois, 2023. https://www.proquest.com/docview/2791530898/abstract/61D166D4666042B4PQ/1 (accessed 2023−11−21).
(20) Centellas, P. J.; Yourdkhani, M.; Vyas, S.; Koohbor, B.; Geubelle, P. H.; Sottos, N. R. Rapid Multiple-Front Polymerization of Fiber-Reinforced Polymer Composites. *Compos. Part Appl. Sci. Manuf.* **2022**, *158*, No. 106931.
(21) Goli, E.; Robertson, I. D.; Geubelle, P. H.; Moore, J. S. Frontal Polymerization of Dicyclopentadiene: A Numerical Study. *J. Phys. Chem. B* **2018**, *122* (16), 4583−4591.
(22) Gao, Y.; Shaon, F.; Kumar, A.; Bynum, S.; Gary, D.; Sharp, D.; Pojman, J. A.; Geubelle, P. H. Rapid Frontal Polymerization Achieved with Thermally Conductive Metal Strips. *Chaos Interdiscip. J. Nonlinear Sci.* **2021**, *31* (7), No. 073113.
(23) Mariani, A.; Bidali, S.; Fiori, S.; Sangermano, M.; Malucelli, G.; Bongiovanni, R.; Priola, A. UV-Ignited Frontal Polymerization of an Epoxy Resin. *J. Polym. Sci. Part Polym. Chem.* **2004**, *42* (9), 2066−2072.
(24) Sangermano, M.; D'Anna, A.; Marro, C.; Klikovits, N.; Liska, R. UV-Activated Frontal Polymerization of Glass Fibre Reinforced Epoxy Composites. *Compos. Part B Eng.* **2018**, *143*, 168−171.
(25) Nason, C.; Pojman, J. A.; Hoyle, C. The Effect of a Trithiol and Inorganic Fillers on the Photo-Induced Thermal Frontal Polymerization of a Triacrylate. *J. Polym. Sci. Part Polym. Chem.* **2008**, *46* (24), 8091−8096.
(26) Stawiasz, K. J.; Wendell, C. I.; Suslick, B. A.; Moore, J. S. Photoredox-Initiated Frontal Ring-Opening Metathesis Polymerization. *ACS Macro Lett.* **2022**, *11* (6), 780−784.
(27) Nason, C.; Roper, T.; Hoyle, C.; Pojman, J. A. UV-Induced Frontal Polymerization of Multifunctional (Meth)Acrylates. *Macromolecules* **2005**, *38* (13), 5506−5512.
(28) Stawiasz, K. J.; Paul, J. E.; Schwarz, K. J.; Sottos, N. R.; Moore, J. S. Photoexcitation of Grubbs' Second-Generation Catalyst Initiates Frontal Ring-Opening Metathesis Polymerization. *ACS Macro Lett.* **2020**, *9* (11), 1563−1568.
(29) Dean, L. M.; Ravindra, A.; Guo, A. X.; Yourdkhani, M.; Sottos, N. R. Photothermal Initiation of Frontal Polymerization Using Carbon Nanoparticles. *ACS Appl. Polym. Mater.* **2020**, *2* (11), 4690−4696.
(30) Liu, Y.; Wang, C.-F.; Chen, S. Facile Access to Poly-(DMAEMA-Co-AA) Hydrogels via Infrared Laser-Ignited Frontal Polymerization and Their Polymerization in the Horizontal Direction. *RSC Adv.* **2015**, *5* (39), 30514−30521.
(31) Zhou, Z.-F.; Yu, C.; Wang, X.-Q.; Tang, W.-Q.; Wang, C.-F.; Chen, S. Facile Access to Poly(NMA-Co-VCL) Hydrogels via Long Range Laser Ignited Frontal Polymerization. *J. Mater. Chem. A* **2013**, *1* (25), 7326−7331.
(32) Li, Q.; Zhang, W.; Wang, C.-F.; Chen, S. In Situ Access to Fluorescent Dual-Component Polymers towards Optoelectronic Devices via Inhomogeneous Biphase Frontal Polymerization. *RSC Adv.* **2015**, *5* (124), 102294−102299.
(33) Fan, S.; Liu, S.; Wang, X.-Q.; Wang, C.-F.; Chen, S. Laser-Ignited Frontal Polymerization of Shape-Controllable Poly(VI-Co-AM) Hydrogels Based on 3D Templates toward Adsorption of Heavy Metal Ions. *Appl. Phys. A: Mater. Sci. Process.* **2016**, *122* (6), 599.
(34) Xie, T.; Nowak, A. P.; BOUNDY, T. Formulations, Methods, and Apparatus for Remote Triggering of Frontally Cured Polymers. US10174223B2, January 8, 2019. https://patents.google.com/patent/US10174223B2/en?oq=US10174223 (accessed 2024−02−08).
(35) Winter, L. G. *The Inverse Problem to the Voronoi Diagram*. Thesis, 2007. https://twu-ir.tdl.org/handle/11274/12058 (accessed 2023−09−19).

https://doi.org/10.1021/acsami.4c00216
ACS Appl. Mater. Interfaces XXXX, XXX, XXX−XXX

(36) Schaer, G.; Bretl, T. Closed-Loop Control of Front Speed During Frontal Polymerization of Dicyclopentadiene—A Numerical Study. *Adv. Theory Simul.* **2023**, *6* (8), 2300015.

https://doi.org/10.1021/acsami.4c00216
ACS Appl. Mater. Interfaces XXXX, XXX, XXX−XXX